Journal of Scientific Computing (2020) 83:7
https://doi.org/10.1007/s10915-020-01174-4

New Finite Difference Hermite WENO Schemes for Hamilton–Jacobi Equations

Jun Zhu[1] · **Feng Zheng**[2] · **Jianxian Qiu**[2]

Received: 23 April 2019 / Revised: 17 February 2020 / Accepted: 21 February 2020

Abstract
In this paper, new finite difference Hermite weighted essentially non-oscillatory (HWENO) schemes are designed for solving the Hamilton–Jacobi equations on structured meshes. The crucial idea of the spatial reconstructions is borrowed from the original HWENO schemes (Qiu and Shu in J Comput Phys 204:82–99, 2005), in which the function and its first derivative values are evolved in time and used in the reconstruction. Such new HWENO spatial reconstructions with the application of three unequal-sized spatial stencils result in an important innovation that we perform only spatial HWENO reconstructions for numerical fluxes of function values and high-order linear reconstructions for numerical fluxes of derivatives, which are different to other HWENO schemes. The new HWENO schemes could obtain smaller errors with optimal high-order accuracy in smooth regions, and keep sharp transitions and non-oscillatory property near discontinuities. Extensive benchmark examples are performed to illustrate the good performance of such new finite difference HWENO schemes.

Keywords HWENO scheme · Unequal-sized spatial stencil · High-order linear reconstruction · HWENO reconstruction · Hamilton–Jacobi equation

Mathematics Subject Classification 65M60 · 35L65

The research is partly supported by Science Challenge Project, No. TZ2016002 and NSFC Grant 11872210, 11571290 and NSAF Grant U1630247. J. Zhu: The author was partly supported by NSFC Grant 11826104 when he visited Tianyuan Mathematical Center in Southeast China, Xiamen, Fujian 361005, P.R. China.

✉ Jianxian Qiu
jxqiu@xmu.edu.cn

Jun Zhu
zhujun@nuaa.edu.cn

Feng Zheng
fzbz200808-31@163.com

1 College of Science, Nanjing University of Aeronautics and Astronautics, Nanjing 210016, Jiangsu, People's Republic of China

2 School of Mathematical Sciences and Fujian Provincial Key Laboratory of Mathematical Modeling and High-Performance Scientific Computing, Xiamen University, Xiamen 361005, Fujian, People's Republic of China

Published online: 19 March 2020

1 Introduction

In this paper, new Hermite weighted essentially non-oscillatory (HWENO) schemes are presented for solving the Hamilton–Jacobi equations

$$\begin{cases} \phi_t + H(\nabla_x \phi) = 0, \\ \phi(x, 0) = \phi_0(x), \end{cases} \tag{1.1}$$

in which $x = (x_1, \ldots, x_n)^T$ are n-spatial variables. Such Hamilton–Jacobi equations often arise in the applications of image processing, geometric optics, material science, computer vision, and so on [8,21,32]. Although the exact solution $\phi(x_1, \ldots, x_n, t)$ for simulating (1.1) is continuous, its derivatives might contain discontinuities. Since it is well known that many Hamilton–Jacobi equations are multi-solution equations, we should apply the physical implications to obtain their viscosity solutions uniquely [1].

Because the Hamilton–Jacobi equations are of close relationship with the conservation laws, we often solve the Hamilton–Jacobi equations with the aid of techniques developed for the conservation laws. So the classical numerical schemes for simulating the conservation laws can be directly adapted or with minor modifications for solving the Hamilton–Jacobi equations. Crandall and Lion [10] proposed first-order monotone schemes and analyzed that the schemes can converge to the viscosity solutions. Although such monotone schemes are only first-order accuracy, they are the building blocks for designing higher order numerical schemes. Following such principles, Osher et al. [24,25] designed some high-order accurate essentially non-oscillatory (ENO) schemes for solving the Hamilton–Jacobi equations. Lafon and Osher [17] constructed ENO schemes for solving the Hamilton–Jacobi equations on unstructured meshes. Then Jiang and Peng [14] proposed classical high-order finite difference weighted ENO (WENO) schemes for solving the Hamilton–Jacobi equations on structured meshes, which are excellent expanding application of the basic fifth-order finite difference WENO schemes [15] for the conservation laws. Some high-order WENO schemes et al. [15,20,26,38] were also designed for two-dimensional Hamilton–Jacobi equations with the application of the nodal WENO-type algebraic polynomial interpolations on unstructured meshes. Hermite WENO (HWENO) schemes [27,30,39,42] were proposed to use more compact spatial stencils for obtaining the same order of accuracy in smooth regions. Bryson and Levy [4] designed central schemes for solving the Hamilton–Jacobi equations. Above mentioned high-order schemes are mainly designed in the finite difference framework. And there are many high-order schemes designed in the finite volume or discontinuous Galerkin (DG) framework. These schemes can be defined on structured or unstructured meshes. A new methodology of DG method for the conservation laws with modification to solve for the Hamilton–Jacobi equations was proposed by Hu and Shu [13]. After that, Cheng and Shu [9] designed direct DG methods for solving the Hamilton–Jacobi equations for $\phi(x_1, \ldots, x_n, t)$ with some remedy procedures originated from [13] in some extreme cases. Yan and Osher [36] proposed a local DG method for directly solving the Hamilton–Jacobi equations with auxiliary variables. And Qiu et al. [27–30,39,41] devoted their efforts to construct the compact Hermite WENO schemes whose solutions and first-order derivative values are applied to compute the conservation laws and the Hamilton–Jacobi equations successfully. Some classical HWENO schemes et al. [5,6,22,23,35,37] were also designed for solving the hyperbolic conservation laws effectively. One major advantage of HWENO schemes superior to WENO schemes is their compactness in spatial reconstruction procedures. We do remark that all existing HWENO schemes are more costly in computation and storage than that of the same order accurate WENO schemes with the same computational meshes, since the solution and

its derivatives need to be stored and evolved in time. So our main objective is to propose a new type of spatial reconstruction methodologies to remedy such drawback in this paper.

This paper is mainly based on [27,30,39] and is of interest to study the high-order simulation methods for the Hamilton–Jacobi equations with some developments. It obeys the basic reconstruction principles of HWENO schemes in [28,29] and is a direct extension of [44] from the finite difference WENO framework to finite difference HWENO framework. Here we emphasize that the new HWENO schemes are very efficient and could keep good convergence property, since spatial HWENO reconstructions and high-order linear reconstructions are also used in this paper. But the spatial HWENO reconstructions are used all the way in any other HWENO schemes [5,6,22,23,27–30,35,37,39,41]. And it is also shown that the new HWENO schemes could efficiently get smaller truncation errors in all accuracy test cases in comparison with that specified in [30,39]. Generally speaking, we mention a few features and advantages of such new HWENO schemes: the linear weights can be set as any positive numbers on condition that their sum is one; they can be easily extended to multi-dimensions; the HWENO spatial reconstructions with three unequal-sized spatial stencils and high-order linear reconstructions are applied here, which are very different to other HWENO schemes [27,30,39].

The organization of this paper is as follows. In Sect. 2, we review and construct new finite difference HWENO schemes in detail for solving the Hamilton–Jacobi equations in one and two dimensions. Extensive numerical results are proposed in Sect. 3 to illustrate the simplicity, accuracy, and efficiency of these new spatial reconstruction procedures. Concluding remarks are given in Sect. 4.

2 The Design of New Finite Difference HWENO Scheme

In this section, we give new finite difference HWENO schemes for solving the Hamilton–Jacobi equations in one and two dimensions in detail.

2.1 One-Dimensional Finite Difference HWENO Scheme

The governing equation (1.1) is studied in one dimension. For simplicity, we assume that the grid points $\{x_i\}$ are uniform with $x_{i+1} - x_i = h$, and cell $I_i = [x_i - h/2, x_i + h/2]$. Define $u(x,t) = \phi_x(x,t)$ and take into account the first-order derivative of (1.1) in one dimension, the conservation laws are obtained as

$$\begin{cases} u_t + H(u)_x = 0, \\ u(x,0) = u_0(x). \end{cases} \tag{2.1}$$

We define $\phi_i(t) = \phi(x_i,t)$ and $u_i(t) = \phi_x(x_i,t)$, and we have the following system of equations:

$$\begin{cases} \frac{d\phi_i(t)}{dt} = -H(u(x_i,t)), \\ \frac{du_i(t)}{dt} = -H_1(u(x_i,t))u_x|_{x=x_i}. \end{cases} \tag{2.2}$$

We replace $H(u(x_i,t))$ by the numerical flux $\tilde{H}_i$ which is defined as

$$\tilde{H}_i = H\left(\frac{u_i^- + u_i^+}{2}\right) - \frac{\alpha}{2}(u_i^+ - u_i^-). \tag{2.3}$$

In (2.2), $H_1(u(x,t)) = \frac{dH}{du}$. For stability, we also split $H_1(u(x_i,t))$ into a positive part and a negative part locally, denoted by $H^+_{1,i}$ and $H^-_{1,i}$, respectively, and approximate u_x by upwind method. Then (2.2) is approximated by

$$\begin{cases} \frac{d\phi_i(t)}{dt} = -\tilde{H}_i, \\ \frac{du_i(t)}{dt} = -H^+_{1,i}u^-_{x,i} - H^-_{1,i}u^+_{x,i}. \end{cases} \tag{2.4}$$

In which

$$H^-_{1,i} = \frac{1}{2}\left(H_1\left(\frac{u_i^- + u_i^+}{2}\right) - |H_1\left(\frac{u_i^- + u_i^+}{2}\right)|\right), \tag{2.5}$$

and

$$\hat{H}^+_{1,i} = \frac{1}{2}\left(H_1\left(\frac{u_i^- + u_i^+}{2}\right) + |H_1\left(\frac{u_i^- + u_i^+}{2}\right)|\right), \tag{2.6}$$

where $u_i^{\pm}$, and $u_{x,i}^{\pm}$ are the left and right limits of the point values of $u(x_i,t)$ and $u_x(x_i,t)$, respectively. For simplicity, the variable t is omitted in the following, if it does not cause confusion. The method of lines ODE (2.4) is rewritten as

$$\frac{d}{dt}w(t) = L(w). \tag{2.7}$$

Then a third-order TVD Runge-Kutta time discretization method [34]

$$\begin{cases} w^{(1)} = w^n + \triangle t L(w^n), \\ w^{(2)} = \frac{3}{4}w^n + \frac{1}{4}w^{(1)} + \frac{1}{4}\triangle t L(w^{(1)}), \\ w^{n+1} = \frac{1}{3}w^n + \frac{2}{3}w^{(2)} + \frac{2}{3}\triangle t L(w^{(2)}), \end{cases} \tag{2.8}$$

is applied to solve for (2.7) and obtain fully discrete scheme both in space and time.

Since the reconstruction procedure is the key component, we will reconstruct the point values $\{u_i^{\pm}\}$ and $\{u_{x,i}^{\pm}\}$ from $\{\phi_i\}$ and $\{u_i\}$, respectively. The reconstruction procedure should obtain high-order accurate in smooth regions and keep essentially non-oscillatory property in non-smooth regions. This reconstruction procedure is outlined for the fifth-order case in the following.

Algorithm 1 *The procedure to reconstruct* $\{u_i^-\}$.

Step 1 Select a big central spatial stencil $T_1 = \{x_{i-2}, x_{i-1}, x_i, x_{i+1}\}$, which is a combination of four points. Then we construct a Hermite quintic polynomial $p_1(x)$ satisfying

$$p_1(x_j) = \phi_j,\ j = i-2, i-1, i, i+1, \tag{2.9}$$

and

$$p_1'(x_j) = u_j,\ \ j = i-1, i+1. \tag{2.10}$$

Its first-order derivative function at x_i is

$$p_1'(x_i) = -\frac{18\phi_{i-1} + \phi_{i-2} - 9\phi_i - 10\phi_{i+1} + 9hu_{i-1} + 3hu_{i+1}}{18h}. \tag{2.11}$$

Step 2 Select two smaller biased spatial stencils $T_2 = \{x_{i-2}, x_{i-1}, x_i\}$ and $T_3 = \{x_{i-1}, x_i, x_{i+1}\}$, which are combinations of three points, respectively. Then we construct two quadratic polynomials $p_2(x)$ and $p_3(x)$ satisfying

$$p_2(x_j) = \phi_j,\ j = i-2, i-1, i, \tag{2.12}$$

and

$$p_3(x_j) = \phi_j,\ j = i-1, i, i+1. \tag{2.13}$$

Their first-order derivative functions at x_i are

$$p_2'(x_i) = \frac{-4\phi_{i-1} + \phi_{i-2} + 3\phi_i}{2h}, \tag{2.14}$$

and

$$p_3'(x_i) = \frac{-\phi_{i-1} + \phi_{i+1}}{2h}. \tag{2.15}$$

Remark 1 Comparing with [30,39], we select one big central stencil T_1 and two smaller biased stencils T_2 and T_3 for constructing three polynomials. Only three nodal point values of ϕ are used to obtain quadratic polynomials $p_2(x)$ and $p_3(x)$ with respect to the target point x_i, which means no point values of the derivative values of ϕ are introduced in comparison with that in [27,30,39]. By performing such new HWENO spatial reconstruction procedures, it is the first time that we apply the information of ϕ and u to get high-order approximation in smooth regions and only apply the information of ϕ without introducing any u to keep essentially non-oscillatory property in non-smooth regions.

Step 3 With the similar idea of proposed by Levy et al. [18,19] for central WENO schemes, we rewrite $p_1'(x_i)$ as

$$p_1'(x_i) = \gamma_1 \left(\frac{1}{\gamma_1} p_1'(x_i) - \sum_{\ell=2}^{3} \frac{\gamma_\ell}{\gamma_1} p_\ell'(x_i) \right) + \sum_{\ell=2}^{3} \gamma_\ell p_\ell'(x_i). \tag{2.16}$$

Clearly, (2.16) holds for arbitrary $\gamma_1 \neq 0$, we would like to take positive linear weights γ_1, γ_2, and γ_3 on condition that $\sum_{\ell=1}^{3} \gamma_\ell$=1. Following the practice in [12,40,42,43,45], for example, we set one type of the linear weights as $\gamma_1 = 0.98$ and γ_2=γ_3=0.01 in this paper.

Step 4 Compute the smoothness indicators β_n, which measure how smooth the functions $p_n'(x)$ are near the target point x_i. The smaller these smoothness indicators, the smoother the functions are near the target point. We use the similar recipe for the smoothness indicators as in [2,15,38]:

$$\beta_n = \sum_{\alpha=2}^{r} \int_{I_i} h^{2\alpha-3} \left(\frac{d^\alpha p_n(x)}{dx^\alpha} \right)^2 dx, n = 1, 2, 3. \tag{2.17}$$

r equals five for $n = 1$ and r equals two for $n = 2, 3$, respectively.

Step 5 Compute the nonlinear weights based on the linear weights and the smoothness indicators. For instance, as shown in [3,7,11], we use new τ which is simply defined as the absolute difference between β_1, β_2, and β_3. So the associated difference expansions in Taylor series at x_i are

$$\tau = \left(\frac{|\beta_1 - \beta_2| + |\beta_1 - \beta_3|}{2} \right)^2 = O(h^6), \tag{2.18}$$

$$\omega_n = \frac{\bar{\omega}_n}{\sum_{\ell=1}^{3} \bar{\omega}_\ell}, \quad \bar{\omega}_n = \gamma_n \left(1 + \frac{\tau}{\varepsilon + \beta_n} \right), \quad n = 1, 2, 3. \tag{2.19}$$

Here ε is a small positive number to avoid the denominator to become zero. It is easy to verify

$$\frac{\tau}{\varepsilon + \beta_n} = O(h^4), n = 1, 2, 3, \tag{2.20}$$

under the condition $\varepsilon \ll \beta_n$. Therefore, the nonlinear weights ω_n satisfy the order accuracy conditions $\omega_n = \gamma_n + O(h^4)$ [3,7], providing the formal fifth-order accuracy to the WENO scheme in [14,15,33]. We take $\varepsilon = 10^{-6}$ in our computation.

Step 6 The final nonlinear HWENO reconstruction of u_i^- is defined by a convex combination of three reconstructed polynomial approximations

$$u_i^- = \omega_1 \left(\frac{1}{\gamma_1} p_1'(x_i) - \sum_{\ell=2}^{3} \frac{\gamma_\ell}{\gamma_1} p_\ell'(x_i) \right) + \sum_{\ell=2}^{3} \omega_\ell p_\ell'(x_i). \tag{2.21}$$

The reconstruction to u_i^+ is mirror symmetric with respect to x_i of the above procedure.

Remark 2 The terms on the right hand side of (2.21) serve a very crucial role in this paper. Our primary objective is to use a high-degree polynomial to obtain a high-order approximation in smooth regions and use the HWENO procedures to rely on linear polynomials to keep essentially non-oscillatory property near discontinuities. The total number of polynomials is no more than that of the same order finite difference HWENO schemes [39], and the choice of the linear weights is flexible.

Then we reconstruct the approximations of $u_{x,i}^{\pm}$ with the high-order linear reconstructions instead of the HWENO reconstructions from the left and right sides of the point x_i.

Algorithm 2 *The procedure to reconstruct* $\{u_{x,i}^-\}$.

We select a big spatial stencil $Q = \{x_{i-2}, x_{i-1}, x_i, x_{i+1}\}$, which is a combination of four points. Then we construct a Hermite sixth degree polynomial $q(x)$ satisfying

$$q(x_j) = \phi_j, \; j = i-2, \ldots, i+1, \tag{2.22}$$

and

$$q'(x_j) = u_j, \;\; j = i-1, i, i+1. \tag{2.23}$$

Its second-order derivative function at x_i is explicitly formulated as

$$q''(x_i) = \frac{\phi_{i-2} + 54\phi_{i-1} - 81\phi_i + 26\phi_{i+1} + 18hu_{i-1} + 18hu_i - 6hu_{i+1}}{18h^2}. \tag{2.24}$$

Its linear reconstruction of $u_{x,i}^-$ is defined as

$$u_{x,i}^- = q''(x_i). \tag{2.25}$$

Associated linear reconstruction to $u_{x,i}^+$ is mirror symmetric with respect to x_i of the above procedure.

Remark 3 Generally speaking, we design *Algorithm* 1 by borrowing the original idea proposed in [30] using the information defined on nodal points to obtain a fifth-order approximation at the target point in smooth regions. When there is a discontinuity within the spatial stencil T_1, the information of the high-order polynomial defined on the T_1 is effectively abandoned for the nonlinear weight ω_1 would be small, and the approximation order will automatically switch to second by using the information of the low order polynomial either p_2 or p_3. We directly use high-order linear approximation to the second derivative of ϕ, and in [30,39] the high order HWENO approximation is used for the second derivative of ϕ.

2.2 Two-Dimensional Finite Difference HWENO Scheme

The governing equation (1.1) can be extended to two-dimensional case again. We also define $u = \phi_x$ and $v = \phi_y$, and the first-order derivatives of (1.1) are taken as

$$u_t + H_1(u, v)u_x + H_2(u, v)v_x = 0, \tag{2.26}$$

and

$$v_t + H_1(u, v)u_y + H_2(u, v)v_y = 0. \tag{2.27}$$

We define $H_1(u, v) = \frac{\partial H}{\partial u}$ and $H_2(u, v) = \frac{\partial H}{\partial v}$. The semidiscrete form in two dimensions is

$$\begin{cases} \frac{d\phi_{i,j}(t)}{dt} = -H(u(x_i, y_j, t), v(x_i, y_j, t)), \\ \frac{du_{i,j}(t)}{dt} = -H_1(u(x_i, y_j, t), v(x_i, y_j, t))u_x(x_i, y_j, t) - H_2(u(x_i, y_j, t), v(x_i, y_j, t)v_x(x_i, y_j, t), \\ \frac{dv_{i,j}(t)}{dt} = -H_1(u(x_i, y_j, t), v(x_i, y_j, t))u_y(x_i, y_j, t) - H_2(u(x_i, y_j, t), v(x_i, y_j, t)v_y(x_i, y_j, t). \end{cases} \tag{2.28}$$

Then (2.28) is approximated by

$$\begin{cases} \frac{d\phi_{i,j}(t)}{dt} = -\tilde{H}_{i,j}, \\ \frac{du_{i,j}(t)}{dt} = -H^+_{1,i,j}u^-_{x,i,j} - H^-_{1,i,j}u^+_{x,i,j} - \bar{H}_{2,i,j}v_{x,i,j}, \\ \frac{dv_{i,j}(t)}{dt} = -\bar{H}_{1,i,j}u_{y,i,j} - H^+_{2,i,j}v^-_{y,i,j} - H^-_{2,i,j}v^+_{y,i,j}. \end{cases} \tag{2.29}$$

Where $\tilde{H}$ is Lipschitz continuous monotone fluxes consistent with $H(u, v)$ and the simple Lax–Friedrichs flux (2.3) is applied in two dimensions. $\bar{H}_{1,i,j} = H_1(\frac{u^-_{i,j}+u^+_{i,j}}{2}, \frac{v^-_{i,j}+v^+_{i,j}}{2})$ and $\bar{H}_{2,i,j} = H_2(\frac{u^-_{i,j}+u^+_{i,j}}{2}, \frac{v^-_{i,j}+v^+_{i,j}}{2})$. $H^\pm_1$ and $H^\pm_2$ are the negative and positive parts of H_1 and H_2, which are defined as $H^-_{1,i,j} = \frac{1}{2}(\bar{H}_{1,i,j} - |\bar{H}_{1,i,j}|)$, $H^+_{1,i,j} = \frac{1}{2}(\bar{H}_{1,i,j} + |\bar{H}_{1,i,j}|)$, $H^-_{2,i,j} = \frac{1}{2}(\bar{H}_{2,i,j} - |\bar{H}_{2,i,j}|)$, and $H^+_{2,i,j} = \frac{1}{2}(\bar{H}_{2,i,j} + |\bar{H}_{2,i,j}|)$, respectively. $u^\pm_{i,j}, v^\pm_{i,j}, u^\pm_{x,i,j}$, $v^\pm_{x,i,j}$, $u^\pm_{y,i,j}$, and $v^\pm_{y,i,j}$ are the fifth-order accurate approximations from different directions to the nodal values of $u(x_i, y_j, t)$, $v(x_i, y_j, t)$, $u_x(x_i, y_j, t)$, $v_x(x_i, y_j, t)$, $u_y(x_i, y_j, t)$, and $v_y(x_i, y_j, t)$, respectively. The values of $u^\pm_{i,j}$ and $v^\pm_{i,j}$, and $u^\pm_{x,i,j}$ and $v^\pm_{y,i,j}$ are designed by the one-dimensional procedures of *Algorithm* 1 and *Algorithm* 2, respectively, with the index for the other dimension frozen. We define $u_{y,i,j} = \frac{u^+_{y,i,j}+u^-_{y,i,j}}{2}$ and $v^\pm_{x,i,j} = \frac{v^+_{x,i,j}+v^-_{x,i,j}}{2}$. The reconstruction procedures of $\{u^\pm_{y,i,j}\}$ and $\{v^\pm_{x,i,j}\}$ are narrated in detail as follows.

Algorithm 3 *The procedure to reconstruct* $\{u^-_{y,i,j}\}$ *and* $\{v^-_{x,i,j}\}$.

Select a big spatial stencil $T = \{(x_{i+\ell}, y_{j+\ell\ell})\}$, $\ell = -2, \ldots, 2$, and $\ell\ell = -2, \ldots, 2$, which is a combination of twenty-five points. Then we could construct a polynomial $p(x, y) \in span\{1, (\frac{y-y_j}{h}), (\frac{y-y_j}{h})^2, (\frac{y-y_j}{h})^3, (\frac{y-y_j}{h})^4, (\frac{y-y_j}{h})^5, (\frac{x-x_i}{h}), (\frac{x-x_i}{h})(\frac{y-y_j}{h}), (\frac{x-x_i}{h})(\frac{y-y_j}{h})^2, (\frac{x-x_i}{h})(\frac{y-y_j}{h})^3, (\frac{x-x_i}{h})(\frac{y-y_j}{h})^4, (\frac{x-x_i}{h})(\frac{y-y_j}{h})^5, (\frac{x-x_i}{h})^2, (\frac{x-x_i}{h})^2(\frac{y-y_j}{h}), (\frac{x-x_i}{h})^2(\frac{y-y_j}{h})^2, (\frac{x-x_i}{h})^2(\frac{y-y_j}{h})^3, (\frac{x-x_i}{h})^2(\frac{y-y_j}{h})^4, (\frac{x-x_i}{h})^2(\frac{y-y_j}{h})^5, (\frac{x-x_i}{h})^3, (\frac{x-x_i}{h})^3(\frac{y-y_j}{h}), (\frac{x-x_i}{h})^3(\frac{y-y_j}{h})^2, (\frac{x-x_i}{h})^3(\frac{y-y_j}{h})^3, (\frac{x-x_i}{h})^3(\frac{y-y_j}{h})^4, (\frac{x-x_i}{h})^3(\frac{y-y_j}{h})^5, (\frac{x-x_i}{h})^4, (\frac{x-x_i}{h})^4(\frac{y-y_j}{h}), (\frac{x-x_i}{h})^4(\frac{y-y_j}{h})^2, (\frac{x-x_i}{h})^4(\frac{y-y_j}{h})^3, (\frac{x-x_i}{h})^4(\frac{y-y_j}{h})^4, (\frac{x-x_i}{h})^4(\frac{y-y_j}{h})^5, (\frac{x-x_i}{h})^5, (\frac{x-x_i}{h})^5(\frac{y-y_j}{h}), (\frac{x-x_i}{h})^5(\frac{y-y_j}{h})^2, (\frac{x-x_i}{h})^5(\frac{y-y_j}{h})^3, (\frac{x-x_i}{h})^5(\frac{y-y_j}{h})^4\}$ satisfying

$$\begin{aligned} p(x_k, y_l) &= \phi_{k,l}, \\ (k, l) &= (i + \ell, j + \ell\ell),\ \ell = -2, \ldots, 2,\ \ell\ell = -2, \ldots, 2, \end{aligned} \tag{2.30}$$

$$\begin{aligned} p'_x(x_k, y_l) &= u_{k,l}, \\ (k, l) &= (i-2, j+\ell\ell), \ \ell\ell = -2, \ldots, 2, \end{aligned} \tag{2.31}$$

and

$$\begin{aligned} p'_y(x_k, y_l) &= v_{k,l}, \\ (k, l) &= (i+\ell, j-2), \ \ell = -2, \ldots, 2. \end{aligned} \tag{2.32}$$

Then associated linear reconstruction of $\{u^-_{y,i,j}\}$ is

$$u^-_{y,i,j} \approx p''_{xy}(x_i, y_j), \tag{2.33}$$

and the linear reconstruction of $\{v^-_{x,i,j}\}$ is

$$v^-_{x,i,j} \approx p''_{yx}(x_i, y_j). \tag{2.34}$$

The reconstruction for $\{u^+_{y,i,j}\}$ is mirror symmetric of that for $\{u^-_{y,i,j}\}$ with respect to (x_i, y_j), and the reconstruction for $\{v^+_{x,i,j}\}$ is mirror symmetric of that for $\{v^-_{x,i,j}\}$ with respect to (x_i, y_j), respectively.

Remark 4 Following above mentioned procedure, in comparison with finite difference HWENO schemes [39], the main advantages of the new finite difference HWENO schemes are their new spatial reconstruction procedures, which could apply arbitrary positive linear weights with a minor restriction and without degrading numerical accuracy in smooth regions and suppress spurious oscillations in non-smooth regions via applying new nonlinear weights other than that specified in [30,39].

3 Numerical Tests

In this section, we set CFL number as 0.6, denote new finite difference HWENO schemes as HWENO-ZQ schemes, denote classical HWENO schemes of Zheng et al. [39] as HWENO-ZSQ schemes, and denote classical HWENO schemes of Qiu and Shu [30] as HWENO-QS schemes. For the purpose of testing whether the random choice of the positive linear weights would degrade the optimal fifth-order accuracy of HWENO-ZQ schemes or not, we set different types of the linear weights in one-dimensional and two-dimensional accuracy test cases as: (1) $\gamma_1 = 0.98$ and $\gamma_2 = \gamma_3 = 0.01$; (2) $\gamma_1 = \gamma_2 = \gamma_3 = 1.0/3.0$; (3) $\gamma_1 = 0.01$ and $\gamma_2 = \gamma_3 = 0.495$. And the linear weights are recovered as type (1) for other numerical examples, unless specified otherwise.

Example 3.1 We solve the following nonlinear one-dimensional Hamilton–Jacobi equation:

$$\phi_t - \cos(\phi_x + 1) = 0, \quad -1 < x < 1, \tag{3.1}$$

with the initial condition $\phi(x, 0) = -\cos(\pi x)$ and periodic boundary conditions. We compute the result up to $t = 0.5/\pi^2$. The errors and numerical orders of accuracy are shown in Table 1. The errors and numerical orders of accuracy by the classical HWENO-ZSQ scheme and HWENO-QS scheme are shown in the same table for the purpose of obtaining good comparison. Figure 1 shows that HWENO-ZQ scheme needs less CPU time than that of HWENO-ZSQ scheme and HWENO-QS scheme to obtain the same quantities of L^1 and L^∞ errors, so HWENO-ZQ scheme is more efficient than other two HWENO schemes in this one-dimensional test case. And it is observed that HWENO-ZQ scheme, HWENO-ZSQ scheme, and HWENO-QS scheme could achieve their designed order of accuracy in smooth regions.

Table 1 $\phi_t - \cos(\phi_x + 1) = 0.\ \phi(x, 0) = -\cos(\pi x)$

Grid points	L^1 error	Order	L^∞ error	Order	L^1 error	Order	L^∞ error	Order
	HWENO-ZQ (1) scheme				HWENO-ZQ (2) scheme			
100	2.64E–8		3.90E–7		4.61E–8		5.35E–7	
120	1.03E–8	5.16	1.62E–7	4.80	1.40E–8	6.52	1.62E–7	6.56
140	4.84E–9	4.90	7.38E–8	5.12	5.80E–9	5.73	7.38E–8	5.10
160	2.54E–9	4.84	3.88E–8	4.81	2.79E–9	5.49	3.83E–8	4.92
180	1.40E–9	5.02	2.17E–8	4.93	1.49E–9	5.28	2.15E–8	4.90
	HWENO-ZQ (3) scheme							
100	5.58E–8		7.86E–7					
120	1.59E–8	6.88	2.28E–7	6.78				
140	6.30E–9	6.01	7.39E–8	7.32				
160	2.92E–9	5.77	3.80E–8	4.98				
180	1.54E–9	5.40	2.13E–8	4.88				
	HWENO-ZSQ scheme				HWENO-QS scheme			
100	2.73E–8		2.49E–7		9.70E–8		2.81E–6	
120	1.17E–8	4.66	1.52E–7	4.55	4.28E–8	4.48	1.32E–6	4.14
140	5.30E–9	5.14	9.41E–8	3.12	2.06E–8	4.75	6.69E–7	4.42
160	2.64E–9	5.20	5.49E–8	4.04	1.06E–8	4.94	3.59E–7	4.65
180	1.49E–9	4.89	3.18E–8	4.64	5.81E–9	5.15	2.03E–7	4.85

Periodic boundary conditions. $T = 0.5/\pi^2$

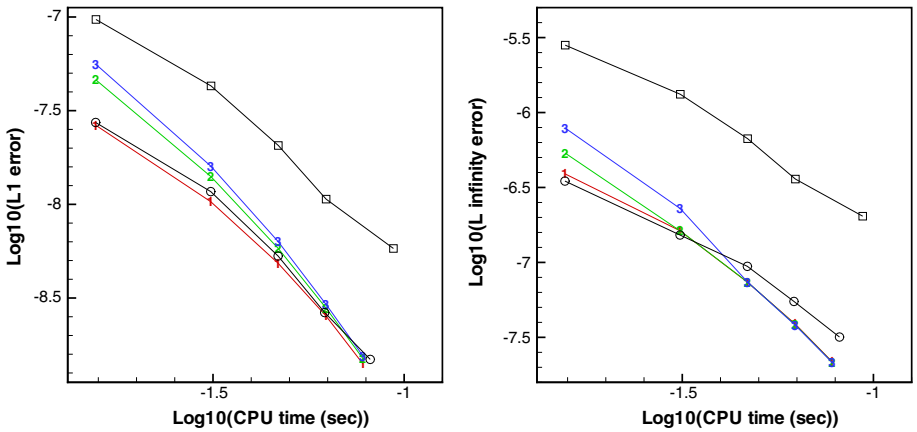

Fig. 1 $\phi_t - \cos(\phi_x + 1) = 0.\ \phi(x, 0) = -\cos(\pi x)$. Computing time and error. Number signs and a solid line denote the results of HWENO-ZQ scheme with different linear weights (1), (2), and (3); circles and a solid line denote the results of HWENO-ZSQ scheme; squares and a solid line denote the results of HWENO-QS scheme

Example 3.2 We solve two-dimensional Burgers' equation:

$$\phi_t + \frac{(\phi_x + \phi_y + 1)^2}{2} = 0, \quad -2 \le x, y < 2, \tag{3.2}$$

Table 2 $\phi_t + \frac{(\phi_x+\phi_y+1)^2}{2} = 0$. $\phi(x, y, 0) = -\cos(\pi(x+y)/2)$. Periodic boundary conditions. $T = 0.5/\pi^2$

	HWENO-ZQ (1) scheme				HWENO-ZQ (2) scheme			
Grid points	L^1 error	Order	L^∞ error	Order	L^1 error	Order	L^∞ error	Order
100×100	8.10E-9		3.72E-8		2.10E-8		2.91E-7	
120×120	3.18E-9	5.13	1.50E-8	4.97	5.59E-9	7.27	6.16E-8	8.51
140×140	1.46E-9	5.05	7.22E-9	4.76	2.02E-9	6.59	1.53E-8	9.03
160×160	7.44E-10	5.04	3.64E-9	5.13	8.95E-10	6.10	4.08E-9	9.90
180×180	4.11E-10	5.03	2.07E-9	4.79	4.60E-10	5.65	2.07E-9	5.76
	HWENO-ZQ (3) scheme							
Grid points	L^1 error	Order	L^∞ error	Order				
100×100	2.77E-8		4.34E-7					
120×120	6.88E-9	7.65	9.30E-8	8.45				
140×140	2.34E-9	6.98	2.36E-8	8.90				
160×160	9.93E-10	6.44	6.55E-9	9.60				
180×180	4.93E-10	5.94	2.16E-9	9.40				
	HWENO-ZSQ scheme				HWENO-QS scheme			
Grid points	L^1 error	Order	L^∞ error	Order	L^1 error	Order	L^∞ error	Order
100×100	3.34E-8		4.51E-7		5.81E-8		7.94E-7	
120×120	1.31E-8	5.13	1.92E-7	4.70	2.32E-8	5.03	3.22E-7	4.95
140×140	6.13E-9	4.94	8.85E-8	5.01	1.09E-8	4.87	1.50E-7	4.94
160×160	3.17E-9	4.94	4.51E-8	5.06	5.80E-9	4.76	7.54E-8	5.17
180×180	1.75E-9	5.03	2.45E-8	5.17	3.30E-9	4.79	4.10E-8	5.18

with the initial condition $\phi(x, y, 0) = -\cos(\pi(x + y)/2)$ and periodic boundary conditions. The final time is $t = 0.5/\pi^2$ and the solution is still smooth at that time. The errors and numerical orders of accuracy by the HWENO-ZQ scheme, HWENO-ZSQ scheme, and HWENO-QS scheme are shown in Table 2, respectively. The numerical errors against CPU time graphs are presented in Fig. 2. It is obvious that HWENO-ZQ scheme needs less CPU time than the results of HWENO-ZSQ scheme and HWENO-QS scheme to obtain the same quantities of L^1 and L^∞ errors, so HWENO-ZQ scheme is more efficient than other two HWENO schemes in this two-dimensional test case.

Example 3.3 We solve the following two-dimensional Hamilton–Jacobi equation:

$$\phi_t - \cos(\phi_x + \phi_y + 1) = 0, \quad -2 \le x, y < 2, \tag{3.3}$$

with the initial condition $\phi(x, y, 0) = -\cos(\pi(x + y)/2)$ and periodic boundary conditions in two directions. The final time is $t = 0.5/\pi^2$. The errors and numerical orders of accuracy by the HWENO-ZQ scheme with different linear weights in comparison with that of HWENO-ZSQ scheme and HWENO-QS scheme are shown in Table 3 and the numerical errors against CPU time graphs are in Fig. 3. HWENO-ZQ scheme with different types of linear weights perform better results than that of other two high-order HWENO schemes in this two-dimensional test case.

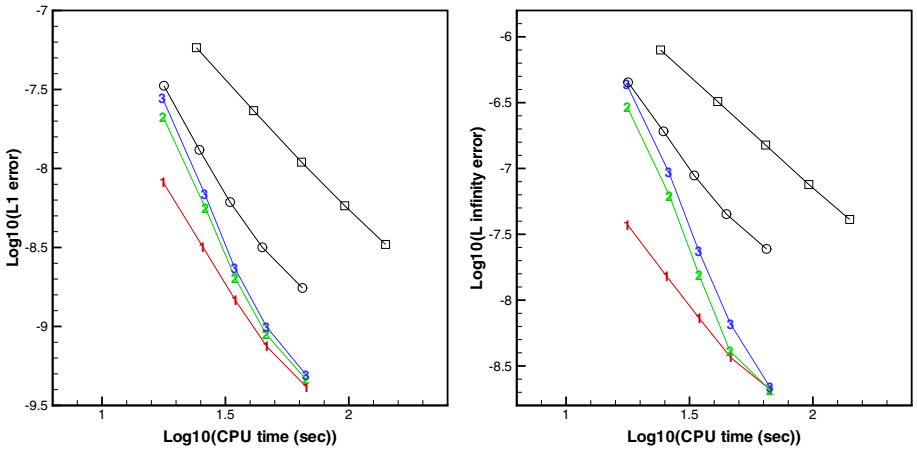

Fig. 2 $\phi_t + \frac{(\phi_x+\phi_y+1)^2}{2} = 0.\ \phi(x, y, 0) = -\cos(\pi(x+y)/2)$. Computing time and error. Number signs and a solid line denote the results of HWENO-ZQ scheme with different linear weights (1), (2), and (3); circles and a solid line denote the results of HWENO-ZSQ scheme; squares and a solid line denote the results of HWENO-QS scheme

Table 3 $\phi_t - \cos(\phi_x + \phi_y + 1) = 0.\ \phi(x, y, 0) = -\cos(\pi(x + y)/2)$. Periodic boundary conditions. $T = 0.5/\pi^2$

	HWENO-ZQ (1) scheme				HWENO-ZQ (2) scheme			
Grid points	L^1 error	Order	L^∞ error	Order	L^1 error	Order	L^∞ error	Order
100×100	3.41E-8		4.94E-7		3.62E-8		4.92E-7	
120×120	1.39E-8	4.89	1.82E-7	5.48	1.43E-8	5.07	1.81E-7	5.47
140×140	6.43E-9	5.05	9.29E-8	4.39	6.50E-9	5.14	9.25E-8	4.38
160×160	3.21E-9	5.19	4.90E-8	4.78	3.23E-9	5.23	4.89E-8	4.77
180×180	1.72E-9	5.28	2.56E-8	5.51	1.73E-9	5.31	2.56E-8	5.49
	HWENO-ZQ (3) scheme							
Grid points	L^1 error	Order	L^∞ error	Order				
100×100	3.74E-8		4.90E-7					
120×120	1.45E-8	5.17	1.81E-7	5.46				
140×140	6.54E-9	5.20	9.23E-8	4.38				
160×160	3.24E-9	5.25	4.88E-8	4.77				
180×180	1.73E-9	5.32	2.56E-8	5.47				
	HWENO-ZSQ scheme				HWENO-QS scheme			
Grid points	L^1 error	Order	L^∞ error	Order	L^1 error	Order	L^∞ error	Order
100×100	6.52E-8		1.98E-6		1.05E-7		2.87E-6	
120×120	2.92E-8	4.40	8.84E-7	4.42	4.58E-8	4.60	1.28E-6	4.40
140×140	1.44E-8	4.57	4.33E-7	4.63	2.19E-8	4.76	6.33E-7	4.59
160×160	7.77E-9	4.65	2.28E-7	4.82	1.16E-8	4.77	3.35E-7	4.76
180×180	4.55E-9	4.53	1.26E-7	5.00	6.68E-9	4.70	1.88E-7	4.91

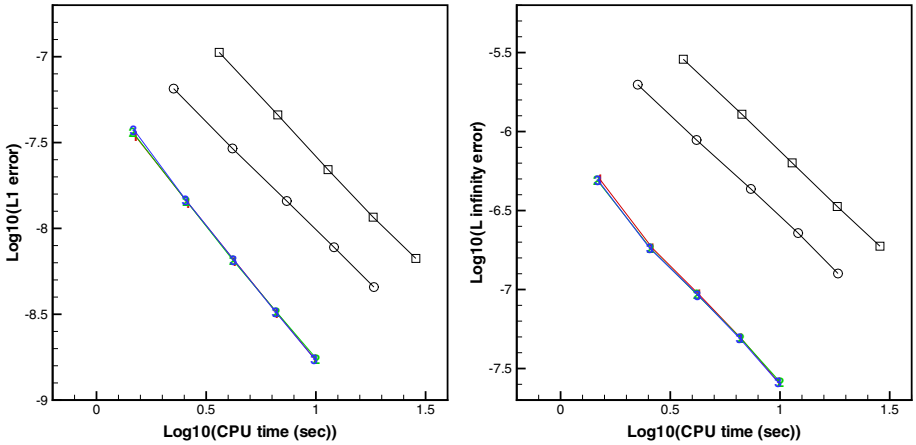

Fig. 3 $\phi_t - \cos(\phi_x + \phi_y + 1) = 0$. $\phi(x, y, 0) = -\cos(\pi(x + y)/2)$. Computing time and error. Number signs and a solid line denote the results of HWENO-ZQ scheme with different linear weights (1), (2), and (3); circles and a solid line denote the results of HWENO-ZSQ scheme; squares and a solid line denote the results of HWENO-QS scheme

Example 3.4 We solve the linear equation:

$$\phi_t + \phi_x = 0, \tag{3.4}$$

with the initial condition $\phi(x, 0) = \phi_0(x - 0.5)$ together with the periodic boundary condition:

$$\phi_0(x) = -(\frac{\sqrt{3}}{2} + \frac{9}{2} + \frac{2\pi}{3})(x + 1) + \begin{cases} 2\cos(\frac{3\pi x^2}{2}) - \sqrt{3}, & -1 \le x < -\frac{1}{3}, \\ \frac{3}{2} + 3\cos(2\pi x), & -\frac{1}{3} \le x < 0, \\ \frac{15}{2} - 3\cos(2\pi x), & 0 \le x < \frac{1}{3}, \\ \frac{28+4\pi+\cos(3\pi x)}{3} + 6\pi x(x-1), & \frac{1}{3} \le x < 1. \end{cases} \tag{3.5}$$

We plot the results with 100 cells at $t = 2$ and $t = 12$ in Fig. 4. It is observed that the results by the HWENO-ZQ scheme have good resolution at the right corner singularity and HWENO-QS scheme gives a bigger offset at the left corner singularity especially at $t = 12$. So we find a fact that the HWENO-ZQ scheme have good resolutions for this benchmark test.

Example 3.5 We solve the one-dimensional nonlinear Burgers' equation:

$$\phi_t + \frac{(\phi_x + 1)^2}{2} = 0, \tag{3.6}$$

with the initial condition $\phi(x, 0) = -\cos(\pi x)$ and the periodic boundary condition. The final time is $t = 3.5/\pi^2$. We find that the discontinuous derivative appears at that time. The solutions of the HWENO-ZQ scheme are given in Fig. 5. We can see the new fifth-order HWENO scheme gives good resolutions for this one-dimensional test.

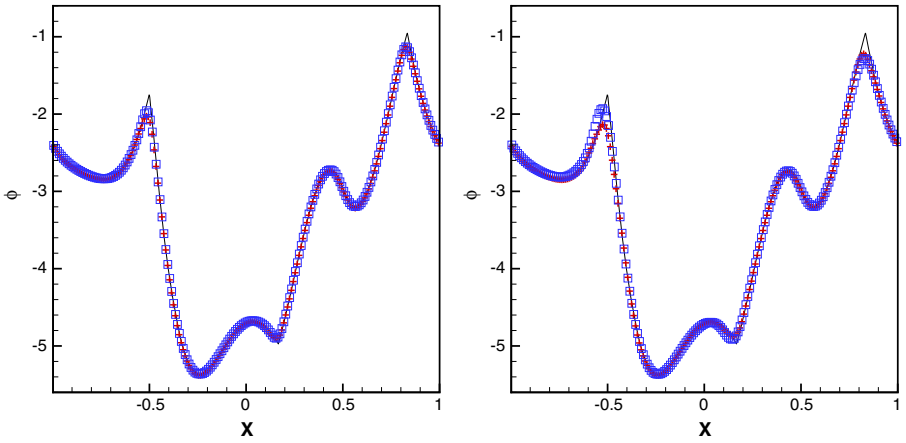

Fig. 4 One-dimensional linear equation. 200 grid points. Left: $t = 2$; right: $t = 12$. Solid line: the exact solution; cross symbols: HWENO-ZQ scheme; square symbols: HWENO-QS scheme

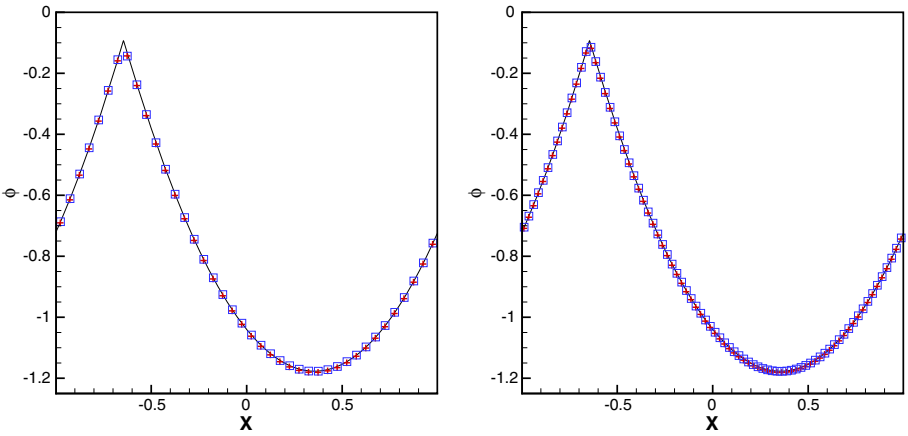

Fig. 5 One-dimensional Burgers' equation. Left: 40 grid points; right: 80 grid points. $T = 3.5/\pi^2$. Solid line: the exact solution; cross symbols: HWENO-ZQ scheme; square symbols: HWENO-QS scheme

Example 3.6 We solve the nonlinear equation with a non-convex flux:

$$\phi_t - cos(\phi_x + 1) = 0, \tag{3.7}$$

with the initial data $\phi(x, 0) = -\cos(\pi x)$ and the periodic boundary condition. The numerical results are plotted at $t = 1.5/\pi^2$ in Fig. 6 when the discontinuous derivative appears. It is observed that the new fifth-order HWENO-ZQ scheme and classical HWENO-QS scheme could obtain similar good results for this problem.

Example 3.7 We solve the one-dimensional Riemann problem with a nonconvex flux:

$$\begin{cases} \phi_t + \frac{1}{4}(\phi_x^2 - 1)(\phi_x^2 - 4) = 0, \quad -1 < x < 1, \\ \phi(x, 0) = -2|x|. \end{cases} \tag{3.8}$$

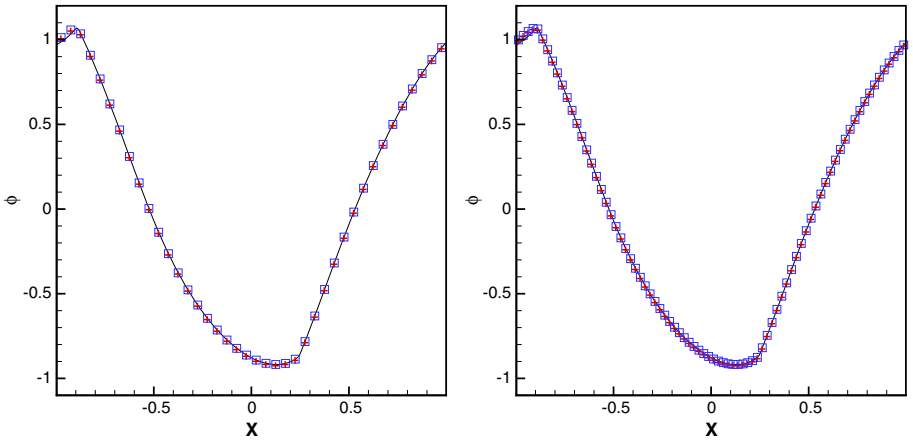

Fig. 6 Problem with the non-convex flux $H(\phi_x) = -\cos(\phi_x + 1)$. Left: 40 grid points; right: 80 grid points. $T = 3.5/\pi^2$. Solid line: the exact solution; cross symbols: HWENO-ZQ scheme; square symbols: HWENO-QS scheme

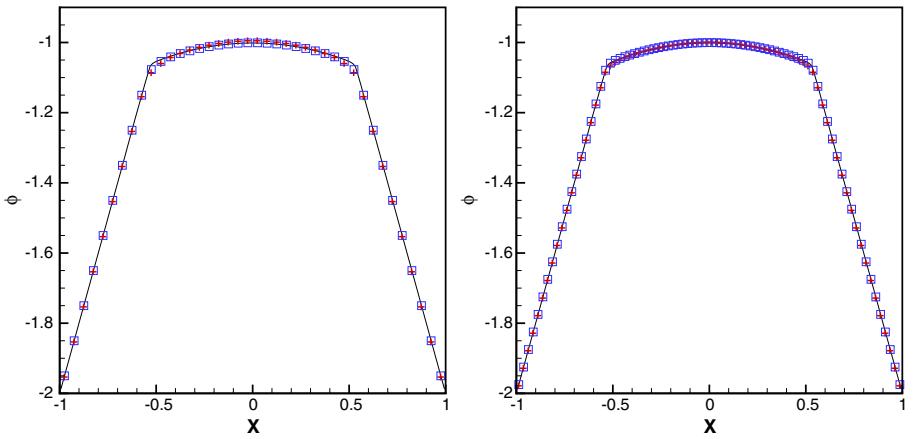

Fig. 7 Problem with the non-convex flux $H(\phi_x) = \frac{1}{4}(\phi_x^2 - 1)(\phi_x^2 - 4)$. Left: 40 grid points; right: 80 grid points. $T = 1$. Solid line: the exact solution; cross symbols: HWENO-ZQ scheme; square symbols: HWENO-QS scheme

It is a demanding test case, because of many high-order schemes have poor resolutions or could even converge to a non-viscosity solution for this example. The final time is t=1 and the numerical results are computed by the HWENO-ZQ scheme with 40 and 80 grid points in Fig. 7, respectively. It is a fact that two fifth-order HWENO schemes could give similar numerical results for this problem.

Example 3.8 We solve the same two-dimensional nonlinear Burgers' equation (3.2) as in Example 3.3 with the same initial condition $\phi(x, y, 0) = -\cos(\pi(x + y)/2)$, except that the results are plotted at $t = 1.5/\pi^2$ in Fig. 8. The discontinuous derivative has already appeared in the solution at that time. It is obvious that the new fifth-order HWENO-ZQ scheme could give good resolutions for this example.

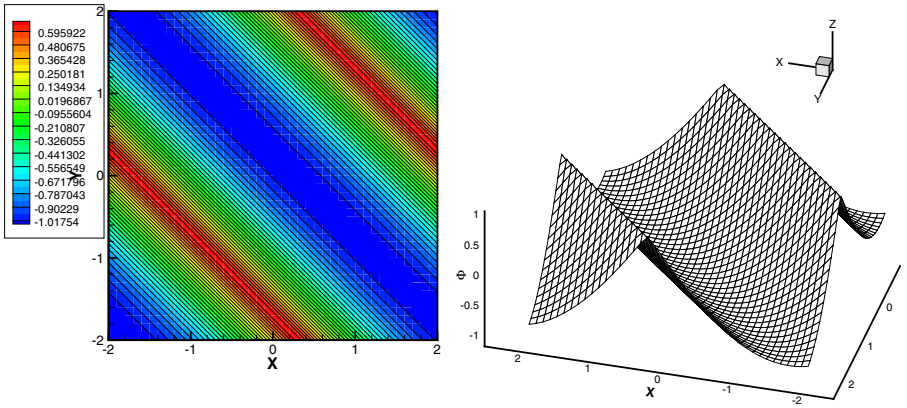

Fig. 8 Two-dimensional Burgers' equation. 40×40 grid points. $T = 1.5/\pi^2$. HWENO-ZQ scheme. Left: contours of the solution; right: the surface of the solution

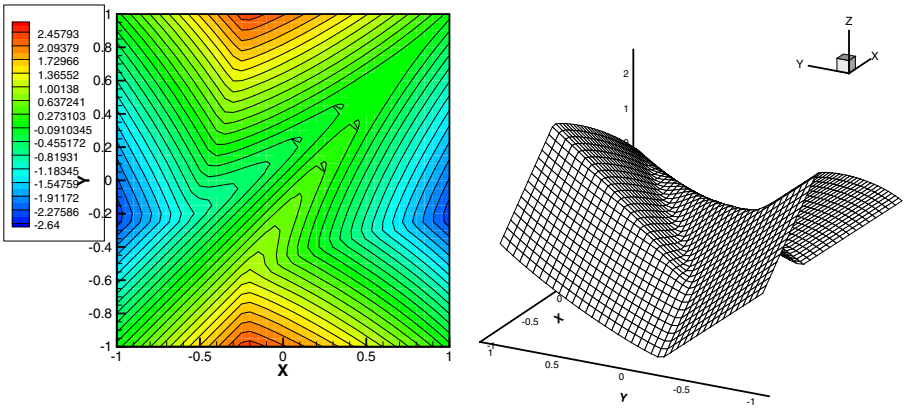

Fig. 9 Two-dimensional Riemann problem with a non-convex flux $H(\phi_x, \phi_y) = \sin(\phi_x + \phi_y)$. 40×40 grid points. $T = 1$. HWENO-ZQ scheme. Left: contours of the solution; right: the surface of the solution

Example 3.9 The two-dimensional Riemann problem with a nonconvex flux:

$$\begin{cases} \phi_t + \sin(\phi_x + \phi_y) = 0, \quad -1 \le x, y < 1, \\ \phi(x, y, 0) = \pi(|y| - |x|). \end{cases} \tag{3.9}$$

For this example, we use a uniform rectangular mesh with 40×40 grid points and associated numerical solutions of the HWENO-ZQ scheme are plotted at $t = 1$ in Fig. 9. We can also observe good numerical results which converge towards an entropy solution.

Example 3.10 A problem from optimal control:

$$\begin{cases} \phi_t + \sin(y)\phi_x + (\sin(x) + sign(\phi_y))\phi_y - \frac{1}{2}\sin^2(y) - (1 - \cos(x)) = 0, \quad \pi < x, y < \pi, \\ \phi(x, y, 0) = 0, \end{cases} \tag{3.10}$$

with periodic conditions in two directions [25]. The solutions of the new fifth-order HWENO-ZQ scheme are plotted at $t = 1$ and the optimal control $\omega = \text{sign}(\phi_y)$ is also shown in Fig. 10.

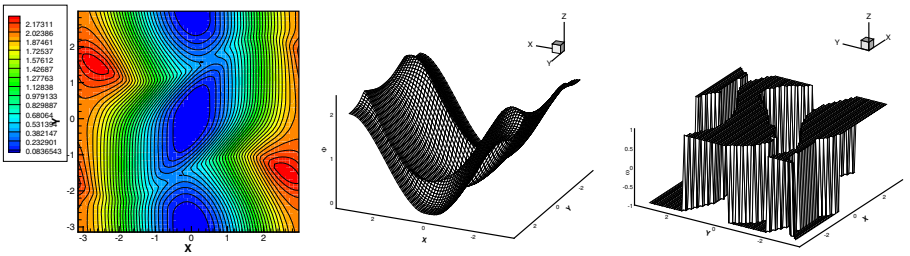

Fig. 10 The optimal control problem. 60×60 grid points. $T = 1$. HWENO-ZQ scheme. From left to right: contours of the solution; the surface of the solution; right: the optimal control $\omega = \text{sign}(\phi_y)$

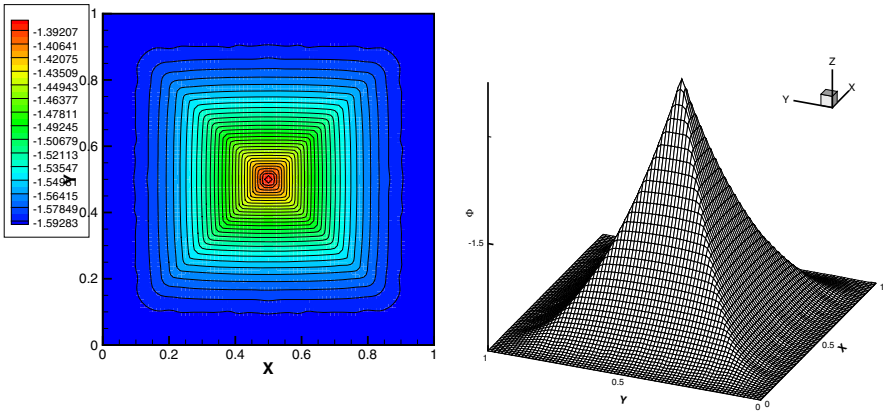

Fig. 11 Eikonal equation with a non-convex Hamiltonian. 80×80 grid points. $T = 0.6$. HWENO-ZQ scheme. Left: contours of the solution; right: the surface of the solution

It is found that such new HWENO scheme could get good numerical resolutions for this two-dimensional test.

Example 3.11 A two-dimensional Eikonal equation with a nonconvex Hamiltonian, which arises in geometric optics [16]:

$$\begin{cases} \phi_t + \sqrt{\phi_x^2 + \phi_y^2 + 1} = 0, \quad 0 \le x, y < 1, \\ \phi(x, y, 0) = \frac{1}{4}(\cos(2\pi x) - 1)(\cos(2\pi y) - 1) - 1, \end{cases} \tag{3.11}$$

The final time is $t = 0.6$. The numerical solutions of the HWENO-ZQ scheme are plotted in Fig. 11. We observe good resolutions of the new fifth-order HWENO scheme for this example.

Example 3.12 A two-dimensional combustion problem [17]:

$$\begin{cases} \phi_t - \sqrt{1 + \phi_x^2 + \phi_y^2} = 0, \quad 0 < x, y < 1, \\ \phi(x, y, 0) = \cos(2\pi x) - \cos(2\pi y). \end{cases} \tag{3.12}$$

The final time is $t = 0.36$. The numerical solution of the HWENO-ZQ scheme is plotted in Fig. 12. We observe good resolutions of the new HWENO-ZQ scheme for this example.

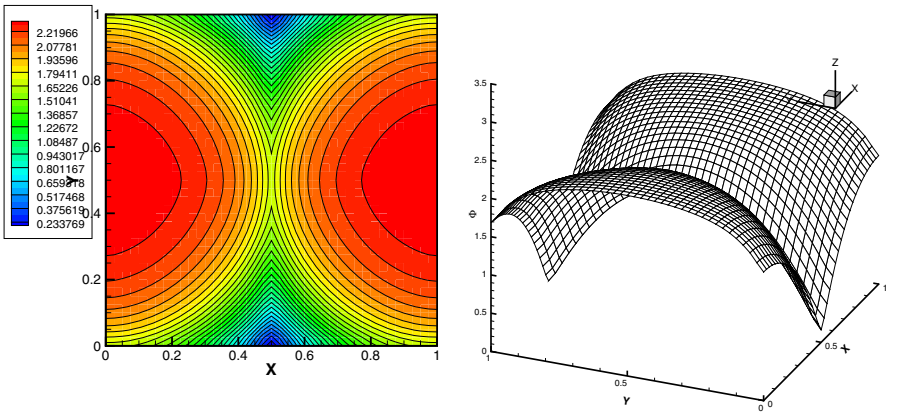

Fig. 12 A combustion problem. 40×40 grid points. $T = 0.36$. HWENO-ZQ scheme. Left: contours of the solution; right: the surface of the solution

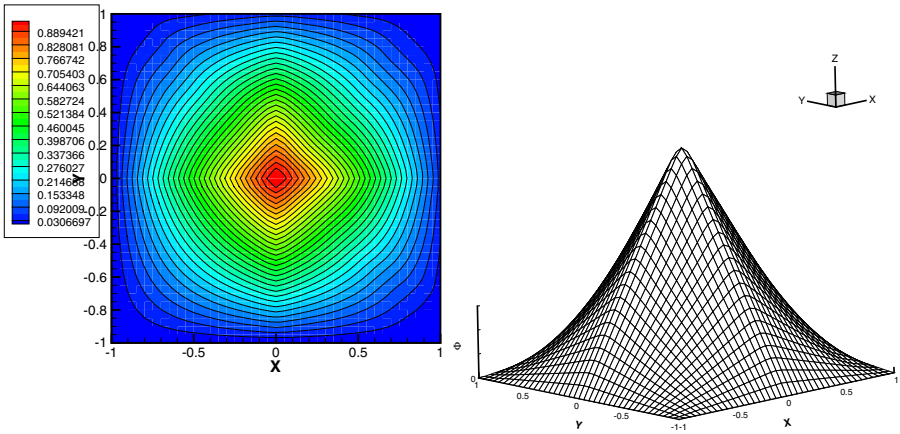

Fig. 13 A computer vision problem. 40×40 grid points. HWENO-ZQ scheme. Left: contours of the solution; right: the surface of the solution

Example 3.13 A problem from computer vision [31] is:

$$\begin{cases} \phi_t + I(x, y)\sqrt{1 + \phi_x^2 + \phi_y^2} - 1 = 0, \quad -1 < x, y < 1, \\ \phi(x, y, 0) = 0, \end{cases} \tag{3.13}$$

in which $I(x, y) = \frac{1}{\sqrt{1+(1-|x|)^2+(1-|y|)^2}}$ together with $\phi = 0$ as the boundary condition. The steady-state solution of this problem is the shape lighted by a source located at infinity with vertical direction. The solution is not unique if there are points at which $I(x, y)$=1 and conditions should be given at those points [38]. The exact steady solution is $\phi(x, y, \infty) = (1-|x|)(1-|y|)$. The numerical solution of the HWENO-ZQ scheme is plotted in Fig. 13. We observe good resolutions of the new HWENO-ZQ scheme for this benchmark steady-state problem.

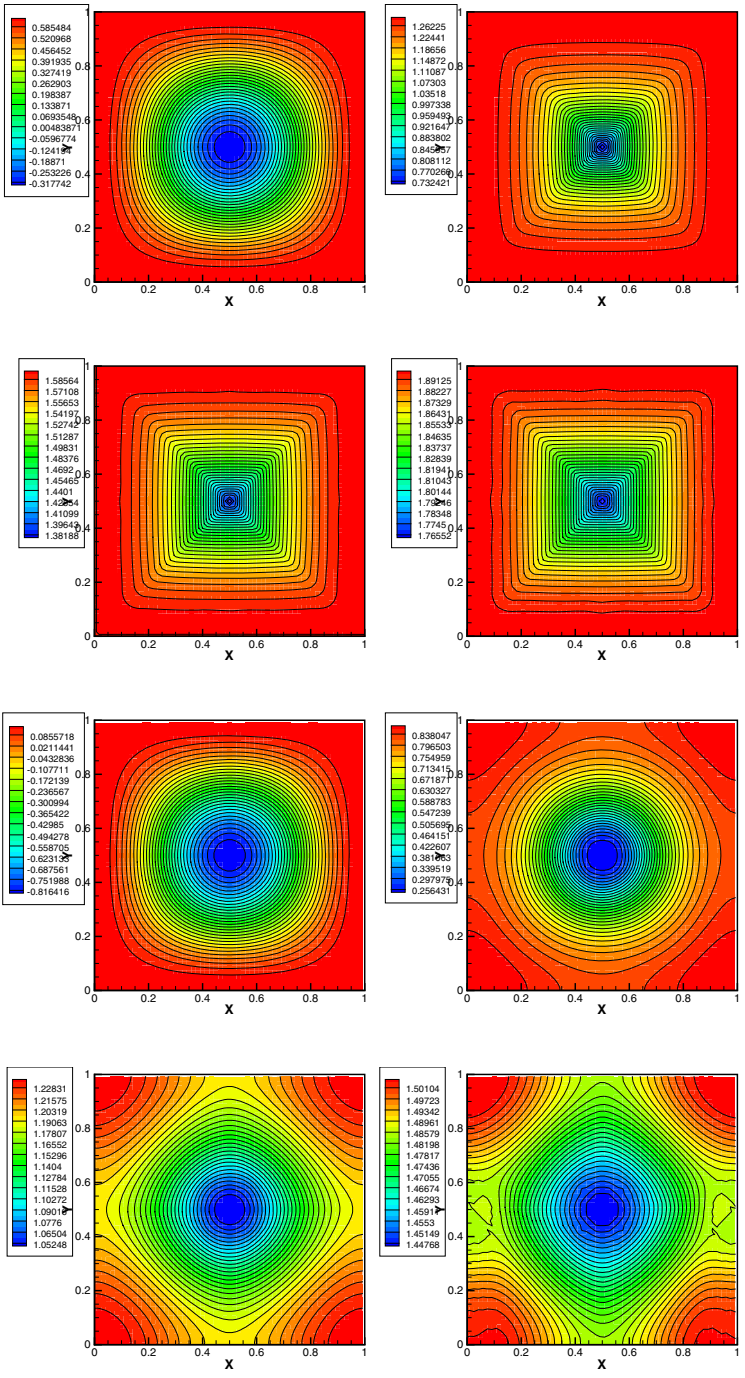

Fig. 14 Propagating surface. 60×60 grid points. From left to right and top to bottom: contours of the solution with $\varepsilon = 0$ at t=0, t=0.3, t=0.6, and t=0.9; contours of the solution with $\varepsilon = 0.1$ at t=0, t=0.1, t=0.3, and t=0.6. HWENO-ZQ scheme

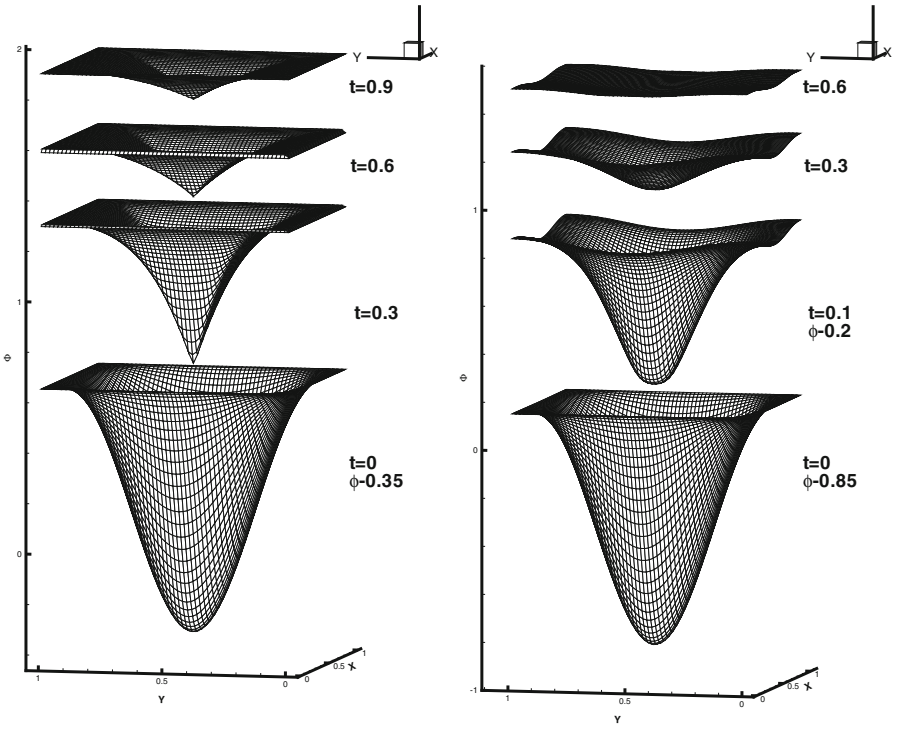

Fig. 15 Propagating surface. 60×60 grid points. Left: $\varepsilon = 0$; right: $\varepsilon = 0.1$. HWENO-ZQ scheme

Example 3.14 The problem of a propagating surface [24]:

$$\begin{cases} \phi_t - (1 - \varepsilon K)\sqrt{\phi_x^2 + \phi_y^2 + 1} = 0, \quad 0 \le x, y < 1, \\ \phi(x, y, 0) = 1 - \frac{1}{4}(\cos(2\pi x) - 1)(\cos(2\pi y) - 1), \end{cases} \tag{3.14}$$

where K is the mean curvature defined by:

$$K = -\frac{\phi_{xx}(1 + \phi_y)^2 - 2\phi_{xy}\phi_x\phi_y + \phi_{yy}(1 + \phi_x^2)}{(1 + \phi_x^2 + \phi_y^2)^{3/2}},$$

and ε is a small constant. A periodic boundary conditions are used in different directions, respectively. The approximation of K is constructed by the methods similar to the first-order derivative terms and three different second order derivatives of associated Hermite reconstruction polynomials are needed. The results of $\varepsilon = 0$ (pure convection) and $\varepsilon = 0.1$ by HWENO-ZQ scheme are presented in Figs. 14 and 15, respectively. The surfaces at $t = 0$ for $\varepsilon = 0$ and for $\varepsilon = 0.1$, and at $t = 0.1$ for $\varepsilon = 0.1$ are shifted downward in order to show the detail of the solution at later time. It is observed that the new fifth-order HWENO-ZQ scheme could get good resolutions for this example with different ε numbers.

4 Concluding Remarks

In this paper, we design new finite difference HWENO schemes for simulating the Hamilton–Jacobi equations in one and two dimensions on structured meshes. The constructions of such HWENO schemes are based on new Hermite interpolation with a series of unequal-sized spatial stencils and a third-order TVD Runge-Kutta time discretization method [34]. The original idea of the spatial reconstructions for the HWENO schemes comes from [27–30]. In designing such new HWENO schemes, the solution and its first derivatives are evolved and used in the HWENO reconstructions and high-order linear reconstructions, respectively, in contrast to the classical HWENO schemes [27–30,39,41] where only the HWENO reconstructions are used. Comparing with all the other existing HWENO schemes et al. [27–30,39,41], the major advantages of such new HWENO schemes are their simplicity, effectiveness, and could fast converge to non-viscosity solutions.

References

1. Abgrall, R., Sonar, T.: On the use of Muehlbach expansions in the recovery step of ENO methods. Numer. Math. **76**, 1–25 (1997)
2. Balsara, D.S., Rumpf, T., Dumbser, M., Munz, C.D.: Efficient, high accuracy ADER-WENO schemes for hydrodynamics and divergence-free magnetohydrodynamics. J. Comput. Phys. **228**, 2480–2516 (2009)
3. Borges, R., Carmona, M., Costa, B., Don, W.S.: An improved weighted essentially non-oscillatory scheme for hyperbolic conservation laws. J. Comput. Phys. **227**, 3191–3211 (2008)
4. Bryson, S., Levy, D.: High-order semi-discrete central-upwind schemes for multi-dimensional Hamilton–Jacobi equations. J. Comput. Phys. **189**, 63–87 (2003)
5. Capdeville, G.: A Hermite upwind WENO scheme for solving hyperbolic conservation laws. J. Comput. Phys. **227**, 2430–2454 (2008)
6. Capdeville, G.: Hermite upwind positive schemes (HUPS) for non-linear hyperbolic systems of conservation laws. Comput. Fluids **156**, 421–440 (2017)
7. Castro, M., Costa, B., Don, W.S.: High order weighted essentially non-oscillatory WENO-Z schemes for hyperbolic conservation laws. J. Comput. Phys. **230**, 1766–1792 (2011)
8. Chan, C.K., Lau, K.S., Zhang, B.L.: Simulation of a premixed turbulent Name with the discrete vortex method. Int. J. Numer. Methods Eng. **48**, 613–627 (2000)
9. Cheng, Y.D., Shu, C.-W.: A discontinuous Galerkin finite element method for directly solving the Hamilton–Jacobi equations. J. Comput. Phys. **223**, 398–415 (2007)
10. Crandall, M., Lions, P.L.: Two approximations of solutions of Hamilton–Jacobi equations. Math. Comput. **43**, 1–19 (1984)
11. Don, W.S., Borges, R.: Accuracy of the weighted essentially non-oscillatory conservative finite difference schemes. J. Comput. Phys. **250**, 347–372 (2013)
12. Dumbser, M., Käser, M.: Arbitrary high order non-oscillatory finite volume schemes on unstructured meshes for linear hyperbolic systems. J. Comput. Phys. **221**, 693–723 (2007)
13. Hu, C., Shu, C.-W.: A discontinuous Galerkin finite element method for Hamilton–Jacobi equations. SIAM J. Sci. Comput. **21**, 666–690 (1999)
14. Jiang, G.S., Peng, D.: Weighted ENO schemes for Hamilton–Jacobi equations. SIAM J. Sci. Comput. **21**, 2126–2143 (2000)
15. Jiang, G.S., Shu, C.-W.: Efficient implementation of weighted ENO schemes. J. Comput. Phys. **126**, 202–228 (1996)
16. Jin, S., Xin, Z.: Numerical passage from systems of conservation laws to Hamilton–Jacobi equations, and relaxation schemes. SIAM J. Numer. Anal. **35**, 2163–2186 (1998)
17. Lafon, F., Osher, S.: High order two dimensional nonoscillatory methods for solving Hamilton–Jacobi scalar equations. J. Comput. Phys. **123**, 235–253 (1996)
18. Levy, D., Puppo, G., Russo, G.: Central WENO schemes for hyperbolic systems of conservation laws, M2AN. Math. Model. Numer. Anal. **33**, 547–571 (1999)
19. Levy, D., Puppo, G., Russo, G.: Compact central WENO schemes for multidimensional conservation laws. SIAM J. Sci. Comput. **22**(2), 656–672 (2000)

20. Li, X.G., Chan, C.K.: High-order schemes for Hamilton–Jacobi equations on triangular meshes. J. Comput. Appl. Math. **167**, 227–241 (2004)
21. Lions, P.L.: Generalized Solutions of Hamilton–Jacobi Equations. Pitman, London (1982)
22. Liu, H., Qiu, J.: Finite difference Hermite WENO schemes for conservation laws. J. Sci. Comput. **63**, 548–572 (2015)
23. Liu, H., Qiu, J.: Finite difference Hermite WENO schemes for conservation laws, II: an alternative approach. J. Sci. Comput. **66**, 598–624 (2016)
24. Osher, S., Sethian, J.: Fronts propagating with curvature dependent speed: algorithms based on Hamilton–Jacobi formulations. J. Comput. Phys. **79**, 12–49 (1988)
25. Osher, S., Shu, C.-W.: High-order essentially nonoscillatory schemes for Hamilton–Jacobi equations. SIAM J. Numer. Anal. **28**, 907–922 (1991)
26. Qiu, J.: WENO schemes with Lax–Wendroff type time discretizations for Hamilton–Jacobi equations. J. Comput. Appl. Math. **200**, 591–605 (2007)
27. Qiu, J.: Hermite WENO schemes with Lax–Wendroff type time discretizations for Hamilton–Jacobi equations. J. Comput. Math. **25**, 131–144 (2007)
28. Qiu, J., Shu, C.-W.: Hermite WENO schemes and their application as limiters for Runge–Kutta discontinuous Galerkin method: one dimensional case. J. Comput. Phys. **193**, 115–135 (2004)
29. Qiu, J., Shu, C.-W.: Hermite WENO schemes and their application as limiters for Runge–Kutta discontinuous Galerkin method II: two-dimensional case. Comput. Fluids **34**, 642–663 (2005)
30. Qiu, J., Shu, C.-W.: Hermite WENO schemes for Hamilton–Jacobi equations. J. Comput. Phys. **204**, 82–99 (2005)
31. Rouy, E., Tourin, A.: A viscosity solutions approach to shape-from-shading. SIAM J. Numer. Anal. **29**, 867–884 (1992)
32. Sethian, J.A.: Level Set Methods and Fast Marching Methods, Evolving Interface, Computational Geometry, Fluid Mechanics, Computer Vision, and Materials Science. Cambridge University Press, Cambridge (1999)
33. Shu, C.-W.: Essentially non-oscillatory and weighted essentially non-oscillatory schemes for hyperbolic conservation laws, in Advanced Numerical Approximation of Nonlinear Hyperbolic Equations. edited by A. Quarteroni, Editor, Lecture Notes in Mathematics, CIME subseries (*Springer-Verlag, Berlin/New York*); ICASE Report 97-65, (1997)
34. Shu, C.-W., Osher, S.: Efficient implementation of essentially non-oscillatory shock capturing schemes. J. Comput. Phys. **77**, 439–471 (1988)
35. Tao, Z., Li, F., Qiu, J.: High-order central Hermite WENO schemes on staggered meshes for hyperbolic conservation laws. J. Comput. Phys. **281**, 148–176 (2015)
36. Yan, J., Osher, S.: A local discontinuous Galerkin method for directly solving Hamilton–Jacobi equations. J. Comput. Phys. **230**, 232–244 (2011)
37. Zahran, Y.H., Abdalla, A.H.: Seventh order Hermite WENO scheme for hyperbolic conservation laws. Comput. Fluids **131**, 66–80 (2016)
38. Zhang, Y.T., Shu, C.-W.: High-order WENO schemes for Hamilton–Jacobi equations on triangular meshes. SIAM J. Sci. Comput. **24**, 1005–1030 (2003)
39. Zheng, F., Shu, C.-W., Qiu, J.: Finite difference Hermite WENO schemes for the Hamilton–Jacobi equations. J. Comput. Phys. **337**, 27–41 (2017)
40. Zhong, X., Shu, C.-W.: A simple weighted essentially nonoscillatory limiter for Runge–Kutta discontinuous Galerkin methods. J. Comput. Phys. **232**, 397–415 (2013)
41. Zhu, J., Qiu, J.: A class of the fourth order finite volume Hermite weighted essentially non-oscillatory schemes. Science China Ser. A Math. **51**, 1549–1560 (2008)
42. Zhu, J., Qiu, J.: A new fifth order finite difference WENO scheme for solving hyperbolic conservation laws. J. Comput. Phys. **318**, 110–121 (2016)
43. Zhu, J., Qiu, J.: A new type of finite volume WENO schemes for hyperbolic conservation laws. J. Sci. Comput. **73**, 1338–1359 (2017)
44. Zhu, J., Qiu, J.: A new fifth order finite difference WENO scheme for Hamilton–Jacobi equations. Numer. Methods Partial Differ. Equ. **33**, 1095–1113 (2017)
45. Zhu, J., Zhong, X., Shu, C.-W., Qiu, J.-X.: Runge-Kutta discontinuous Galerkin method using a new type of WENO limiters on unstructured meshes. J. Comput. Phys. **248**, 200–220 (2013)